A Novel STATCOM Model for Dynamic Power System Simulations

Luis M. Castro, Enrique Acha, *Senior Member, IEEE*, and Claudio R. Fuerte-Esquivel, *Senior Member, IEEE*

***Abstract*—This paper introduces an advanced model of the STATCOM suitable for steady-state and dynamic simulations of large-scale power systems. It allows for a comprehensive representation of the STATCOM's AC and DC circuits—this is in contrast to current practice where the STATCOM is represented using an equivalent variable voltage source which is not amenable to a proper representation of its DC circuit. The new STATCOM model comprises a voltage source converter (VSC) in series with an LTC transformer. The former is represented by a complex tap-changing transformer whose primary and secondary windings would correspond, in a notional sense, to the VSC's AC and DC buses, respectively. The magnitude and phase angle of the complex tap changer correspond to the amplitude modulation index and the phase shift that would exist in a PWM inverter to enable either reactive power generation or absorption purely by electronic processing of the voltage and current waveforms within the VSC. The numerical technique employed to solve the STATCOM model is the Newton-Raphson method for both operating regimes, the steady-state and the dynamic-state. The latter involves discretization of the STATCOMs and synchronous generators differential equations so that the nonlinear algebraic equations and the discretized differential equations are linearized around a base operating point and assembled together in a unified frame-of-reference for robust iterative solutions.**

***Index Terms*—dynamic power system simulations, FACTS, Newton-Raphson method, STATCOM, VSC.**

I. Introduction

THE power electronics equipment that emerged from the FACTS initiative [1] has a common purpose: to alleviate one or more operational problems at key locations of the power grid. A case in point is the STATCOM which has been designed to provide continuously variable reactive power at its point of connection with the grid, in response to both fast and slow network voltage variations. Its good performance arises from the fast action of the PWM-driven IGBT valves which enable the STATCOM to maintain a smooth voltage profile at its connecting node, even in the face of rather severe disturbances in the power grid. This is so because of its fast VAR supporting function by pure electronic processing, i.e., phase-shifting of the voltage and current waveforms within the voltage source converter. Physically, the STATCOM's VSC is built as a two-level or a multi-level inverter operating on a constant DC voltage. A relatively small capacitor which normally stands at about 10% of its full capacitive range is used to support and stabilize the voltage at its DC bus.

Power electronics is a fast moving field in terms of the design of converter topologies and their controls, semiconductor valves and applications. Paradoxically, there has been limited progress in terms of developing realistic models with which to assess their impact on large-scale power grids. The research reported in this paper bridges the gap in this all-important area of power systems. Early attempts used the concept of a controllable voltage source behind a coupling impedance has been a popular modeling resource to represent the steady-state fundamental frequency operation of the STATCOM [2]. This simple concept explains well the operation of the STATCOM from the standpoint of the AC network but its usefulness is very much reduced when the requirement involves the assessment of variables relating to the STATCOM's DC bus. The situation is very much the same when looking at the dynamic regime of the STATCOM where the standard approach has also been the use of a controllable voltage source [3]–[8]. Such representations change little with respect to that reported in [3] where the power flowing into the equivalent voltage source is used to directly control the DC voltage magnitude—to a greater or lesser extent, the ideal voltage source is treated as the DC bus of the STATCOM. Following this idea, a model where the STATCOM is treated as a controllable reactive current source with a time delay, has been put forward in [9]. Nonetheless, all these models exhibit the same shortcoming, namely, the explicit representation of the STATCOM's DC circuit.

Aiming at alleviating such a key shortcoming, the paper puts forward an enhanced STATCOM model suitable for the steady-state and dynamic regimes of large-scale power grids, which has the following attributes: 1) by making explicit the DC bus representation, the inclusion of a realistic switching loss model becomes feasible as well as the option to include DC loads—this has a direct implication when considering extensions of this model into the realm of VSC-HVDC transmission, which is the subject of a forthcoming publication; 2) it is possible to segregate the overall VSC power losses into conduction and switching power losses; 3) by the same token, in this STATCOM model it becomes possible to separate the VSC power losses from those due to the interfacing LTC coupling transformer.

Manuscript received July 12, 2012; revised November 10, 2012 AND February 26, 2013; accepted March 19, 2013. Date of publication April 23, 2013; date of current version July 18, 2013. The work of L. M. Castro was supported by CONACYT, México. Paper no. TPWRS-00806-2012.

L. M. Castro is with the Electrical Engineering Faculty, Universidad Michoacana de San Nicolás de Hidalgo (UMSNH), Morelia, Michoacán, Mexico, and also with the Department of Electrical Energy Engineering, Tampere University of Technology, Tampere, Finland (e-mail: lcastro@dep.fie.umich.mx).

E. Acha is with the Department of Electrical Energy Engineering, Tampere University of Technology (TUT), Tampere, Finland (e-mail: enrique.acha@tut.fi).

C. R. Fuerte-Esquivel is with the Electrical Engineering Faculty, Universidad Michoacana de San Nicolás de Hidalgo (UMSNH), Morelia, Michoacán, México (e-mail: cfuerte@umich.mx).

Color versions of one or more of the figures in this paper are available online at http://ieeexplore.ieee.org.

Digital Object Identifier 10.1109/TPWRS.2013.2255319

Hence, a new dynamic phasor-based STATCOM model is reported in this paper. This model contrasts with those in current use; it departs from the controllable voltage source concept so far used to represent the VSC, resulting in a far superior modeling flexibility when it comes to representing the DC side of the STATCOM. In the new model the VSC is represented as a complex tap-changing transformer; one where its primary and secondary sides yield quite naturally to the VSC's AC and DC sides, respectively. The VSC's AC terminal combines quite easily with the model of the interfacing transformer to make up the STATCOM model.

The overall dynamic model of the STATCOM presented in this paper is developed in an all-encompassing frame-of-reference where the non-linear algebraic equations of the power system, synchronous generators and STATCOMs are linearized around a base operating point and combined together with the discretized differential equations representing the controls of the STATCOMs and synchronous generators, for unified iterative solutions using the Newton-Raphson method. One such iterative solution is valid for a given point in time and its rate of convergence is quadratic. Moreover, the differential equations are discretized using the implicit trapezoidal method for enhanced numerical stability. This is a time-domain solution where the emphasis is placed on the new dynamic STATCOM model which is comprehensive, quite elegant and yields physical insight.

It should be noticed that the new model put forward is not a switching-based model, such as those used in commercial packages as PSCAD® and SIMULINK® where the PWM pattern is fully emulated together with the switching action of each converter valve. Rather, this model follows the standard way of representing electrical equipment and their controls in large-scale electrical power system modeling and simulations [10]—they are said to be lumped-type models. These models take the approach of representing one full period of the fundamental frequency wave form by a phasor corresponding to the base wave form's frequency. It is likely that this modeling approach may correspond to the concept of average value models widely used in the field of power electronics. Lumped-type models are used in a number of industry-grade commercial packages, such as PowerWorld® and PSS/E®. In the former the VSC is represented as a voltage source through which the AC voltage which incorporates elements of the DC bus but no explicit representation of the DC circuit. On the other hand, the latter represents the STATCOM by a shunt element which injects reactive current to keep the specified voltage, but no DC circuit is available and the modulation index cannot be estimated.

The new STATCOM model is tested in three power networks, the IEEE 9-bus system [11], the New England test system [12] and a large utility-level power system [13].

II. STATCOM Model for Dynamic Analysis

A. Key Physical Characteristics

The STATCOM may be seen to comprise a VSC whose AC terminal is connected to the secondary winding of an LTC transformer which plays the role of an interface between the VSC and the AC power grid and adds a further degree of voltage magnitude controllability. Physically, the VSC is built as a two-level

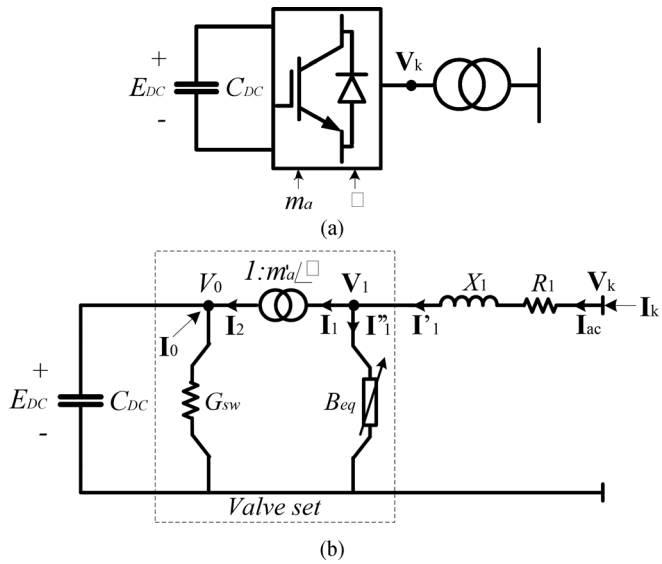

Fig. 1. (a) STATCOM schematic representation. (b) VSC equivalent circuit.

or a multi-level converter that uses an array of self-commutating power electronic switches driven by PWM control. On its DC side, the VSC employs a capacitor bank of small rating whose sole function is to support and stabilise the voltage at its DC bus to enable the converter operation. The converter keeps the capacitor charged to the required voltage level by making its output voltage lag the AC system voltage by a small angle [1]. The DC capacitor of value C_{DC} is shown quite prominently in Fig. 1(a). It should be remarked that C_{DC} is not responsible *per se* for the actual VAR generation process and certainly not at all for the VAR absorption process. Instead the VAR generation/absorption process is carried out by the PWM control which shifts the voltage and current waveforms within the VSC to yield either leading or lagging VAR operation to satisfy operational requirements. Such an electronic processing of the voltage and current waveforms may be well characterized, from the fundamental frequency representation viewpoint, by an equivalent susceptance which can be either capacitive or inductive to conform to operating conditions.

The VSC model comprises an ideal tap changing transformer with complex taps connected in series with an impedance, an equivalent variable shunt susceptance B_{eq} placed on the right-hand side of the transformer and a resistor on its DC side, as seen on Fig. 1(b). The series reactance X_1 represents the VSC's interface magnetics whereas the series resistor R_1 is associated to the ohmic losses which are proportional to the AC terminal current squared. The shunt resistor (with a conductance value of G_{sw}) produces active power losses to account for the switching action of the PWM converter. This conductance is calculated according to the existing operating conditions and ensures that the switching losses be scaled by the quadratic ratio of the actual terminal current I_k to the nominal current I_{nom}

$$G_{sw} = G_0(I_k/I_{nom})^2. \tag{1}$$

The following assumptions are made in the model: 1) the complex voltage $\mathbf{V}_1 = m'_a e^{j\phi} E_{DC}$ is the voltage relative to the system phase reference; 2) the tap magnitude m'_a of the ideal

tap-changing transformer corresponds to the VSC's amplitude modulation coefficient where the following relationship holds for a two-level, three-phase VSC: $m'_a = \sqrt{3}/2 \cdot m_a$; 3) the angle ϕ is the phase angle of voltage $\mathbf{V}_1$; 4) E_{DC} is the DC bus amplitude voltage which is a real scalar and in a per-unit basis carries a value of $\sqrt{2}$.

B. VSC Steady-State Model

The phase-shifting transformer making up the VSC model plays a crucial role in describing the converter operation; it decouples, angle-wise, the circuits connected at both ends of the transformer. Equally important is the fact that the phase angle of the nodal voltage on the left-hand side of the transformer keeps its initialization value, which we may select it to be zero. Hence, if $\theta_0 = 0$ then $\mathbf{V}_0 = V_0 + j0 = V_0$. This has two immediate consequences: from the AC power flow solution point of view, the phase angle of this node is an *a priori* known state variable and the corresponding row and column may be deleted from the Jacobian equation, i.e., it does not need representation; the second consequence is that the AC-DC circuits brought about by the inclusion of one or more STATCOMs in the power network can be solved by using conventional AC power system applications, such as AC power flows. Bearing this in mind, the VSC nodal power flow equations are derived from the admittance matrix developed in Appendix A, as follows:

$$\begin{pmatrix} \mathbf{S}_k \\ \mathbf{S}_0 \end{pmatrix} = \begin{pmatrix} \mathbf{V}_k & \\ & V_0 \end{pmatrix} \times \left\{ \begin{pmatrix} \mathbf{Y}_1^* & -m'_a \angle -\phi \cdot \mathbf{Y}_1^* \\ -m'_a \angle \phi \cdot \mathbf{Y}_1^* & m_a^{'2}(\mathbf{Y}_1^* - jB_{eq}) + G_{sw} \end{pmatrix} \times \begin{pmatrix} \mathbf{V}_k^* \\ V_0 \end{pmatrix} \right\}. \tag{2}$$

After some arduous algebra, the expressions for active and reactive powers injected at both ends of the series branch are arrived at

$$P_k = V_k^2 G_1 - m'_a V_k V_0 [G_1 \cos(\theta_k - \phi) + B_1 \sin(\theta_k - \phi)] \tag{3}$$

$$Q_k = -V_k^2 B_1 - m'_a V_k V_0 [G_1 \sin(\theta_k - \phi) - B_1 \cos(\theta_k - \phi)] \tag{4}$$

$$P_0 = m_a^{'2} V_0^2 G_1 - m'_a V_k V_0 [G_1 \cos(\phi - \theta_k) + B_1 \sin(\phi - \theta_k)] \tag{5}$$

$$Q_0 = -m_a^{'2} V_0^2 B_1 - m'_a V_k V_0 [G_1 \sin(\phi - \theta_k) - B_1 \cos(\phi - \theta_k)]. \tag{6}$$

Additionally, the nodal active and reactive powers for the shunt branches are expressed as follows:

$$P_{sw} = V_0^2 G_0 (I_k / I_{nom})^2 \tag{7}$$

$$Q_{eq} = -m_a^{'2} V_0^2 B_{eq}. \tag{8}$$

Hence, the set of mismatch power flow equations that must be solved to obtain the steady-state equilibrium point is

$$\Delta P_k = -P_k - P_{Lk} - P_k^{cal} \tag{9}$$

$$\Delta Q_k = -Q_k - Q_{Lk} - Q_k^{cal} \tag{10}$$

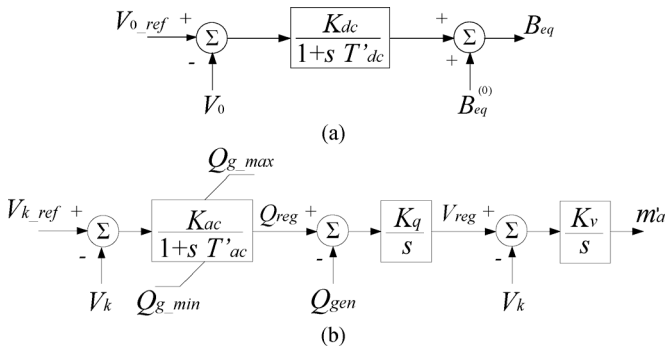

Fig. 2. Dynamic representation of (a) DC-bus controller and (b) AC-bus controller.

$$\Delta P_0 = -P_0 - P_{sw} \tag{11}$$

$$\Delta Q_0 = -Q_0 - Q_{eq} \tag{12}$$

where P_{Lk} and Q_{Lk} represent the active and reactive powers drawn by the load at bus k, respectively, and P_k^{cal} and Q_k^{cal} stand for the powers injected at bus k. They are given by

$$P_k^{cal} = V_k^2 G_{kk} + V_k \sum_{m \in k} V_m [G_{km} \cos(\theta_k - \theta_m) + B_{km} \sin(\theta_k - \theta_m)] \tag{13}$$

$$Q_k^{cal} = -V_k^2 B_{kk} + V_k \sum_{m \in k} V_m [G_{km} \sin(\theta_k - \theta_m) - B_{km} \cos(\theta_k - \theta_m)]. \tag{14}$$

Since the objective is to regulate the voltage magnitude V_k within a specified value and, at the same time, to maintain V_0 at a constant value, the state variables $(\theta_k, m'_a, \phi, B_{eq})$ need to be found by solving (9)–(12). Furthermore, it is necessary to ensure that the VSC operates in the linear range, say, $m_a < 1$. Similarly, the generated reactive power, $Q_{gen} = -Q_k$, must be within the limits: $Q_{g\_\min}$ and $Q_{g\_\max}$.

It is worth mentioning that the STATCOM model is rather flexible and that, if desired, it may take a load on its DC side as illustrated in Section V.

C. VSC Dynamic Model

Modeling of the VSC aimed at dynamic analysis requires two basic controllers, one for the AC side and the other for the DC side, as shown in Fig. 2.

In the control loop shown in Fig. 2(a), the DC voltage magnitude is controlled by B_{eq}. The DC voltage error (the difference between the desired and achieved V_0) together with a first-order controller is used to obtain new values of B_{eq} at every time step. Using this control loop, the DC voltage dynamics is basically determined by the gain K_{dc} and a transient time constant T'_{dc}.

The differential equation that arises from the block diagram corresponding to the DC-bus controller is

$$\frac{dB_{eq}}{dt} = \frac{K_{dc}(V_{0\_ref} - V_0) - B_{eq}}{T'_{dc}}. \tag{15}$$

For the case of the AC-bus controller, the modulation index m'_a is responsible for keeping the voltage magnitude V_{ac} at the desired value, as depicted in Fig. 2(b). This controller is well

represented by three blocks. The first one produces the reference reactive power Q_{reg} after processing the error signal produced by comparing V_k and the reference voltage V_{k_ref}. In the second block the voltage signal V_{reg} is obtained by regulating the error between the VSC's reactive power output Q_{gen} and Q_{reg} with an integrator of gain K_q. In the third block a new value of m'_a is generated by using the actual values of V_k and V_{reg}. Realistic results demand that limits on the reactive power output be taken into account in this controller.

The differential equations for the AC-bus controller are

$$\frac{dQ_{reg}}{dt} = \frac{K_{ac}(V_{k\_ref} - V_k) - Q_{reg}}{T'_{ac}} \tag{16}$$

$$\frac{dV_{reg}}{dt} = K_q(Q_{reg} - Q_{gen}) \tag{17}$$

$$\frac{dm'_a}{dt} = K_v(V_{reg} - V_k). \tag{18}$$

The dynamics of the STATCOM AC and DC buses are modeled using (15)–(18). It should be brought to attention that the dynamic loop of the AC bus shown in Fig. 2(b) shares some similarity with the dynamic loop used in [3] for the same purpose, in the sense that the same state and control variables are employed; even though the two STATCOM representations are fundamentally different. It should be noticed that in contrast to the model presented in Fig. 1(b), the STATCOM model in [3] is an equivalent voltage source. Such a difference in representation yields quite different dynamic loops for the DC bus in this paper and in [3]. In Fig. 2(a), the voltage at the DC bus is regulated by B_{eq} whereas in [3] the state variable is the phase angle of the equivalent voltage source.

III. Dynamic Frame of Reference

Dynamic analysis yields the required information to determine the operating performance of a power system during a disturbance. The power system is very rich in dynamics, encompassing the very fast dynamics due to atmospheric discharges and switching transients, the electro-mechanical oscillations of various kinds and the long-term dynamics due to boiler and turbine controls. Hence, in power systems studies it is normal to develop models of varying degrees of representation to target the phenomena of interest.

In this paper the interest is in assessing the effectiveness of the new STATCOM model to regulate voltage magnitude at its point of connection, following a network topology change such as a change in system load or the tripping of a transmission line or transformer. Hence, the solution method presented in [14] is selected to implement the STATCOM model developed in Section II of this paper. This approach allows combining the set of algebraic equations (19) representing the network with the system of differential equations (20) describing the dynamic behaviour of the machines and their controls, to obtain the solution as a function of time in a unified frame of reference. It makes use of the implicit trapezoidal method (see Appendix B) which is known to be numerically stable, preserving reasonable accuracy, even when the time constants are much smaller than the integration time step [14], [15]

$$0 = f(\mathbf{X}, \mathbf{Y}) \tag{19}$$

$$\dot{y} = g(\mathbf{X}, \mathbf{Y}, t) \tag{20}$$

where $\mathbf{X}$ and $\mathbf{Y}$ are vectors of variables that are computed at discrete points in time.

These equations are efficiently solved using the NR method which possesses strong convergence characteristics. In this case, the conventional power flows Jacobian matrix, $\boldsymbol{J}$, is enlarged to accommodate the partial derivatives that arise from the discretized differential equations and its control variables. The NR method provides an accurate solution to the set of equations given by $f(\boldsymbol{Z}) = 0$, by solving for $\Delta\boldsymbol{Z}$ in the linearized problem $\boldsymbol{J}\Delta\boldsymbol{Z} = -f(\boldsymbol{Z})$ in a repetitive manner. In this case $\boldsymbol{Z}$ is a vector that contains the state variables that emerge from the network, synchronous generators and their controls or any other control device. In an expanded form

$$\begin{bmatrix} \Delta P \\ \Delta Q \\ \hline \Delta F(y) \end{bmatrix} = -\left[\begin{array}{cc|c} \frac{\partial \Delta P}{\partial \theta} & \frac{\partial \Delta P}{\partial V} & \frac{\partial \Delta P}{\partial y} \\ \frac{\partial \Delta Q}{\partial \theta} & \frac{\partial \Delta Q}{\partial V} & \frac{\partial \Delta Q}{\partial y} \\ \hline \frac{\partial F(y)}{\partial \theta} & \frac{\partial F(y)}{\partial V} & \frac{\partial F(y)}{\partial y} \end{array}\right] \begin{bmatrix} \Delta\theta \\ \Delta V \\ \hline \Delta y \end{bmatrix} \tag{21}$$

where ΔP and ΔQ are the active and the reactive power mismatch vectors, respectively; $F(y)$ is a vector that contains the discretized differential equations of each machine or controlling device; $\Delta\theta, \Delta V$ and Δy represent the vectors of incremental changes in nodal voltage angles and magnitudes, as well as the state variables arising from each differential equation. The NR method starts from an initial guess for $\boldsymbol{Z}_0$ and updates the solution at each iteration i, i.e., $\boldsymbol{Z}_{i+1} = \boldsymbol{Z}_i + \Delta\boldsymbol{Z}_i$, until a pre-defined tolerance is fulfilled. In this unified solution, all of the state variables are adjusted simultaneously in order to compute the new equilibrium point of the power system at every time step.

A. Discretization of Differential Equations for the STATCOM Model

The STATCOM differential equations (15)–(18) are discretized and expressed in the form of a mismatch equation in the same fashion as the network's active and reactive power mismatch equations, to enable suitable representation in this unified frame of reference:

1) DC-Bus Controller:

$$F_{B_{eq}} = B_{eq,t-\Delta t} + \frac{\Delta t}{2}\dot{B}_{eq,t-\Delta t} - \left(B_{eq,t} - \frac{\Delta t}{2}\dot{B}_{eq,t}\right) \tag{22}$$

where

$$\dot{B}_{eq,t} = T_{dc}^{'-1}[K_{dc}(V_{0\_ref} - V_{0,t}) - B_{eq,t}] \tag{23}$$

$$\dot{B}_{eq,t-\Delta t} = T_{dc}^{'-1}[K_{dc}(V_{0\_ref} - V_{0,t-\Delta t}) - B_{eq,t-\Delta t}] \tag{24}$$

2) AC-Bus Controller:

$$F_{Q_{reg}} = Q_{reg,t-\Delta t} + \frac{\Delta t}{2}\dot{Q}_{reg,t-\Delta t} - \left(Q_{reg,t} - \frac{\Delta t}{2}\dot{Q}_{reg,t}\right) \tag{25}$$

$$F_{V_{reg}} = V_{reg,t-\Delta t} + \frac{\Delta t}{2}\dot{V}_{reg,t-\Delta t} - \left(V_{reg,t} - \frac{\Delta t}{2}\dot{V}_{reg,t}\right) \tag{26}$$

$$F_{m_a} = m'_{a,t-\Delta t} + \frac{\Delta t}{2}\dot{m}'_{a,t-\Delta t} - \left(m'_{a,t} - \frac{\Delta t}{2}\dot{m}'_{a,t}\right) \tag{27}$$

where

$$\dot{Q}_{reg,t} = T_{ac}^{'-1}[K_{ac}(V_{k\_ref} - V_{k,t}) - Q_{reg,t}] \tag{28}$$

$$\dot{Q}_{reg,t-\Delta t} = T_{ac}^{'-1}[K_{ac}(V_{k\_ref} - V_{k,t-\Delta t}) - Q_{reg,t-\Delta t}] \tag{29}$$

$$\dot{V}_{reg,t} = K_q(Q_{reg,t} - Q_{gen,t}) \tag{30}$$

$$\dot{V}_{reg,t-\Delta t} = K_q(Q_{reg,t-\Delta t} - Q_{gen,t-\Delta t}) \tag{31}$$

$$\dot{m}'_{a,t} = K_v(V_{reg,t} - V_{k,t}) \tag{32}$$

$$\dot{m}'_{a,t-\Delta t} = K_v(V_{reg,t-\Delta t} - V_{k,t-\Delta t}). \tag{33}$$

B. VSC Linearized System of Equations

The expressions (9)–(12), (22) and (25)–(27) make up the set of mismatch equations that must be solved together with the equations of the whole network, for reliable dynamic simulations. The linearized form of the VSC equations is

$$\begin{bmatrix} \Delta P_k \\ \Delta Q_k \\ \Delta P_0 \\ \Delta Q_0 \\ \hline F_{B_0} \\ F_{Q_{reg}} \\ F_{V_{reg}} \\ F_{m_a} \end{bmatrix} = -\left[\begin{array}{c|c} J_{11} & J_{12} \\ \hline J_{21} & J_{22} \end{array}\right] \begin{bmatrix} \Delta\theta_k \\ \Delta V_k \\ \Delta\phi \\ \Delta V_0 \\ \hline \Delta B_{eq} \\ \Delta Q_{reg} \\ \Delta V_{reg} \\ \Delta m'_a \end{bmatrix} \tag{34}$$

where J_{11} comprises the first-order partial derivatives of the nodal active and reactive power mismatches with respect to voltage magnitudes and phase angles of the AC-side as well as the voltage of the DC-side, as shown more explicitly in (35). Likewise, J_{12} in (36) shows the partial derivatives arising from the nodal active and reactive powers with respect to the variables corresponding to the VSC control circuits. The matrix J_{21} consists of partial derivatives of the VSC's discretized differential equations with respect to AC and DC voltages, as shown in (37). Lastly, J_{22} is a matrix that accommodates the first-order partial derivatives of the VSC's discretized differential equations with respect to their control variables, as shown in (38).

C. Initialization of Parameters and Variables

The steady-state equilibrium point that is used to start the dynamic simulation is computed using the conventional NR power flow algorithm, which enables good starting conditions to ensure a suitable dynamic solution. In turns, the NR solution

$$J_{11} = \begin{bmatrix} \frac{\partial\Delta P_k}{\partial\theta_k} & \frac{\partial\Delta P_k}{\partial V_k} & \frac{\partial\Delta P_k}{\partial\phi} & \frac{\partial\Delta P_k}{\partial V_0} \\ \frac{\partial\Delta Q_k}{\partial\theta_k} & \frac{\partial\Delta Q_k}{\partial V_k} & \frac{\partial\Delta Q_k}{\partial\phi} & \frac{\partial\Delta Q_k}{\partial V_0} \\ \frac{\partial\Delta P_0}{\partial\theta_k} & \frac{\partial\Delta P_0}{\partial V_k} & \frac{\partial\Delta P_0}{\partial\phi} & \frac{\partial\Delta P_0}{\partial V_0} \\ \frac{\partial\Delta Q_0}{\partial\theta_k} & \frac{\partial\Delta Q_0}{\partial V_k} & \frac{\partial\Delta Q_0}{\partial\phi} & \frac{\partial\Delta Q_0}{\partial V_0} \end{bmatrix} \tag{35}$$

$$J_{12} = \begin{bmatrix} 0 & 0 & 0 & \frac{\partial\Delta P_k}{\partial m'_a} \\ 0 & 0 & 0 & \frac{\partial\Delta Q_k}{\partial m'_a} \\ 0 & 0 & 0 & \frac{\partial\Delta P_0}{\partial m'_a} \\ \frac{\partial\Delta Q_0}{\partial B_{eq}} & 0 & 0 & \frac{\partial\Delta Q_0}{\partial m'_a} \end{bmatrix} \tag{36}$$

$$J_{21} = \begin{bmatrix} 0 & 0 & 0 & \frac{\partial F_{B_{eq}}}{\partial V_0} \\ 0 & \frac{\partial F_{Q_{reg}}}{\partial V_k} & 0 & 0 \\ \frac{\partial F_{V_{reg}}}{\partial\theta_k} & \frac{\partial F_{V_{reg}}}{\partial V_k} & \frac{\partial F_{V_{reg}}}{\partial\phi} & \frac{\partial F_{V_{reg}}}{\partial V_0} \\ 0 & \frac{\partial F_{m'_a}}{\partial V_k} & 0 & 0 \end{bmatrix} \tag{37}$$

$$J_{22} = \begin{bmatrix} \frac{\partial F_{B_{eq}}}{\partial B_{eq}} & 0 & 0 & 0 \\ 0 & \frac{\partial F_{Q_{reg}}}{\partial Q_{reg}} & 0 & 0 \\ 0 & \frac{\partial F_{V_{reg}}}{\partial Q_{reg}} & \frac{\partial F_{V_{reg}}}{\partial V_{reg}} & \frac{\partial F_{V_{reg}}}{\partial m'_a} \\ 0 & 0 & \frac{\partial F_{m'_a}}{\partial V_{reg}} & \frac{\partial F_{m'_a}}{\partial m'_a} \end{bmatrix} \tag{38}$$

responsible for generating the steady-state equilibrium point is initialized as follows: the amplitude modulation ratio m_a and the angle ϕ are set at 1 and 0, respectively. Also, B_{eq} is initialized at a value that lies within $B_{eq-} = Q_{g\_\min}/V_0$ and $B_{eq+} = Q_{g\_\max}/V_0$.

D. Synchronous Generator and Its Controls, and Loads

The synchronous generator two-axis model may be expressed in terms of four differential equations. The swing equation, given by two first-order differential equations, (39) and (40), describes the motion of the generators' rotor, whereas (41) to (42) define the electrical transient behavior of the rotor circuits, in the dq reference frame:

$$\dot{\omega} = f_\omega(P_m, P_g, \omega, D, H, f_0, \omega_0) \tag{39}$$

$$\dot{\delta} = f_\delta(\omega, \omega_0) \tag{40}$$

$$\dot{E}'_q = f_{E'_q}(E'_q, E_{\rm fd}, I_d, X_d, X'_d, T'_{d0}) \tag{41}$$

$$\dot{E}'_d = f_{E'_d}(E'_d, I_q, X_q, X'_q, T'_{q0}) \tag{42}$$

where T'_{d0}, T'_{q0} are open-circuit transient time constants; E'_d, E'_q are the internal transient flux voltages; E_{fd} is the excitation voltage; I_d, I_q are generators terminal currents; X'_d, X'_q are transient reactances; X_d, X_q are synchronous reactances; H is the inertia constant [s], P_m is the mechanical input power [p.u], P_g is the electrical output power [p.u], D stands for the damping coefficient [s/rad], ω is the synchronous speed [rad/s], f_0 is the system operating frequency [Hz] and δ is the so-called load angle [rad].

A simplified version of the IEEE-type I AVR model [16] is used in this work to regulate the voltage at the generator's terminals through the applied field voltage E_{fd}. In this simplified representation, the saturation function is neglected as well as the transductor function which represents the delay in the measuring of the voltage at the generator's terminal. Also, the feed-back and the exciter blocks in the controller are neglected owing to their very fast dynamics compared to the amplifier block. For the case of the hydroturbine and governor equipment, the models used in our dynamic simulations are shown in [14].

Lastly, the active and reactive powers drawn by the loads are represented by their polynomial representation [17] in which their degree of dependency with respect to their terminal voltage is taken into account.

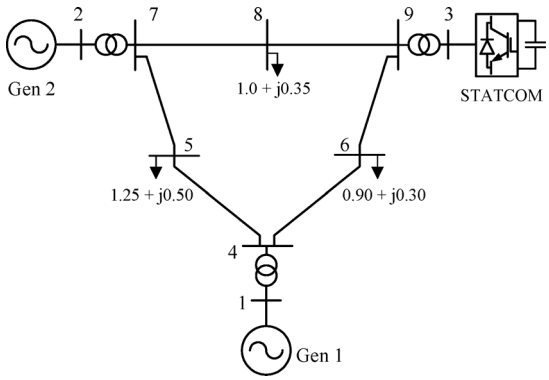

Fig. 3. Test system used to incorporate a STATCOM.

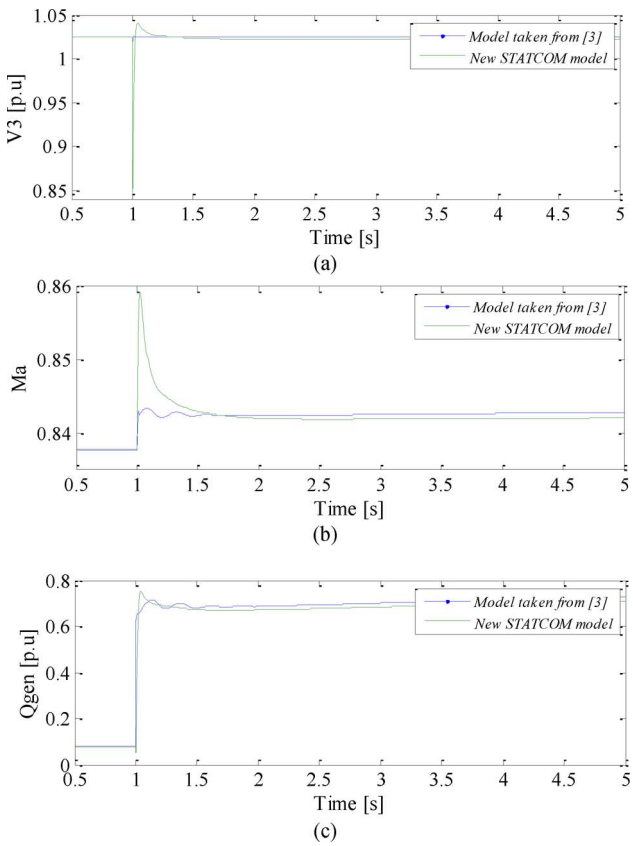

Fig. 4. STATCOM performance during a disturbance. (a) DC-side behavior. (b) AC-side behavior. (c) Reactive power output.

IV. Comparative Study

To validate the new STATCOM model, a comparative study is presented in this section. To that end, the model presented in [3] is used for comparison. The IEEE 9-bus system [11] has been modified slightly, as seen in Fig. 3, where the STATCOM placed at bus 3 provides reactive power support and keeps its terminal voltage at 1.0253 p.u.

The generators connected at nodes 1 and 2 keep their voltages at 1.04 and 1.0253 p.u, respectively. Table I shows the steady-state results for both models where it can be noticed that the inner active power loss and injected reactive power differs significantly. Both models are subject to the same experimental test which consists in tripping the line connecting nodes 7 and 8 at $t = 1$ s. The simulation runs for a total of 5 s with a time step of 10 ms. Following the disturbance, the STATCOM starts taking control over the modulation index and injected reactive power as seen in Fig. 4(b) and (c), respectively. Hence the AC-bus voltage recovers rather quickly as depicted in Fig. 4(a).

TABLE I
Summary of Steady-State Power Flow Results for Both Models

	Model taken from [3]			New STATCOM model		
	Gen 1	*Gen 2*	*STATCOM*	*Gen 1*	*Gen 2*	*STATCOM*
P_g(MW)	158.68	163.0	-2.001	156.64	163.0	-0.012
Q_g(MVAR)	11.32	14.33	8.27	11.23	14.13	7.76
V(p.u)	1.04	1.0253	1.0253	1.04	1.0253	1.0253
M_a	N/A	N/A	0.8378	N/A	N/A	0.8377

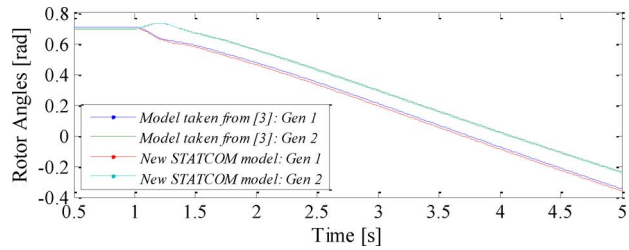

Fig. 5. Generators' rotor angle behavior.

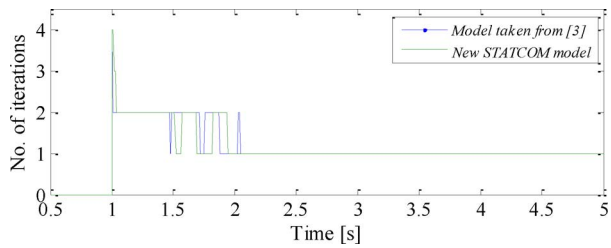

Fig. 6. Number of iterations during the dynamic simulation.

The results of the dynamic simulation shown in Figs. 4 and 5 indicate that the output variables of our model are consistent with those of the voltage source-type model [3], in spite of the fundamentally different modeling approach used. The main numerical differences are due to: 1) the way in which the inner power losses are computed; and 2) the very different control variables that both models use to control key variables at the AC and DC buses.

Convergence is obtained in 5 iterations to a power mismatch tolerance of 10^{-12} for the steady-state solution. To show the prowess of the numerical technique used to solve the new STATCOM model during the dynamic simulation where the tolerance used is 10^{-6}, Fig. 6 shows the number of iterations taken at every time step for both models. It is noticed that for the first second, following the disturbance, the solution method takes two iterations to converge owing to the state and control variables experiencing more significant changes.

By the same token, the maximum number of iterations is taken at the point at which the disturbance occurs. For most of the simulation period, the algorithm takes only one iteration. Note that in spite of the very different nature of the two models, the number of iterations taken at every time step does not vary considerably.

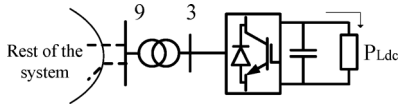

Fig. 7. STATCOM with a constant load on its DC side.

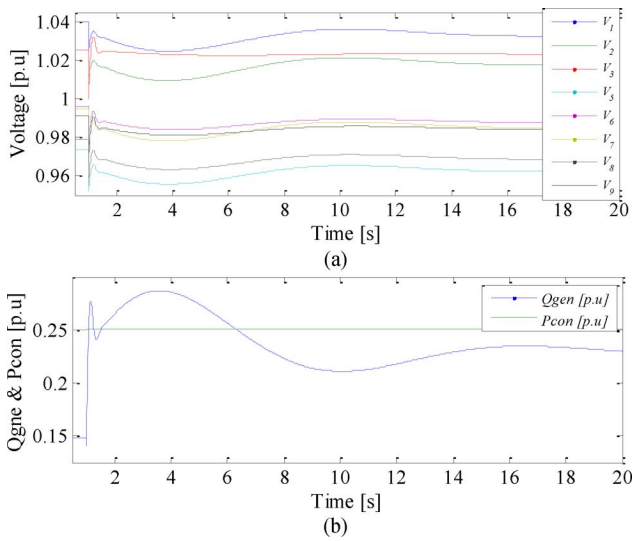

Fig. 8. (a) Voltage performance. (b) Generated reactive power and consumed active power when the VSC is managing a constant load on its DC side.

V. STATCOM Operating With a DC Load

To illustrate the great modeling flexibility afforded by the new STATCOM model, a DC load will be connected to its DC bus, as shown in Fig. 7. The STATCOM is located in the same location in the network presented in Section IV. The constant DC load, P_{Ldc}, carries a value of 0.25 p.u.

In steady-state conditions, the consumed active power, P_{con}, and the reactive power delivered to the grid, Q_{gen}, stand at 25.025 MW and 14.796 MVAr, respectively.

In this case, a load increase of 7% in each load point is simulated at $t = 1$ s. The simulation runs for a total of 20 s. Fig. 10(a) shows the system voltage performance over time at each node of the network. As expected the VSC manages to satisfactorily exert voltage control at the node where the equipment is connected to. Its voltage is maintained practically constant following the disturbance thanks to its reactive power provision, shown in Fig. 8(b). As expected, the DC load is kept constant, as shown in Fig. 8(b), since it has been modeled to be a constant power load.

VI. Study Cases With More Complex Power Networks

In order to test further the performance of the new STATCOM model within a more realistic context in terms of the size of a power network, two test systems are used, namely, the New England system [12] and a large-scale power system [13] which consists of 2172 buses.

A. New England Power System

Fig. 9 depicts the most relevant part of the New England test network, where STATCOMs are placed at nodes 5 and 27. The

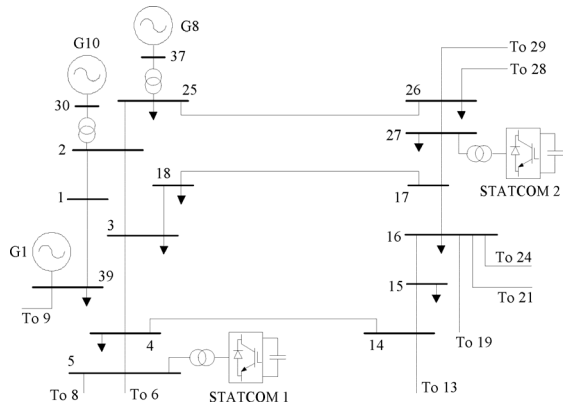

Fig. 9. Relevant area of the New England test system.

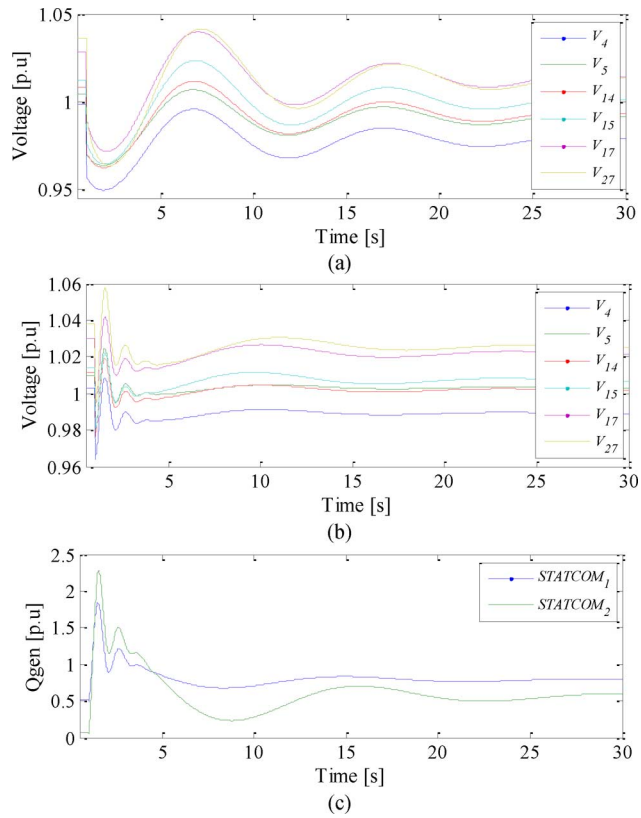

Fig. 10. (a) Voltage behavior with no STATCOMs. (b) Voltage behavior with STATCOMs. (c) Reactive power provided by the STATCOMs.

simulation runs for 30 s, the selected time step is 10 ms and the tolerance used is 10^{-6}.

In this scenario, the transmission lines connecting buses 25-2, 2–3 and 3–4 (which are transmitting about 237 MW, 381 MW and 76 MW, respectively) are tripped at $t = 1$ s. As a consequence, several nodes in the surrounding area experience a significant decrease in voltage magnitude when the STATCOMs are not embedded in the network, as seen on Fig. 10(a). This contrasts with the voltage behavior when the STATCOMs are in operation, as shown in Fig. 10(b), in the sense that the voltages are stabilized much faster. The affected area benefits very substantially during the transient period from the reactive power generated by both STATCOMs, shown in Fig. 10(c). Such a

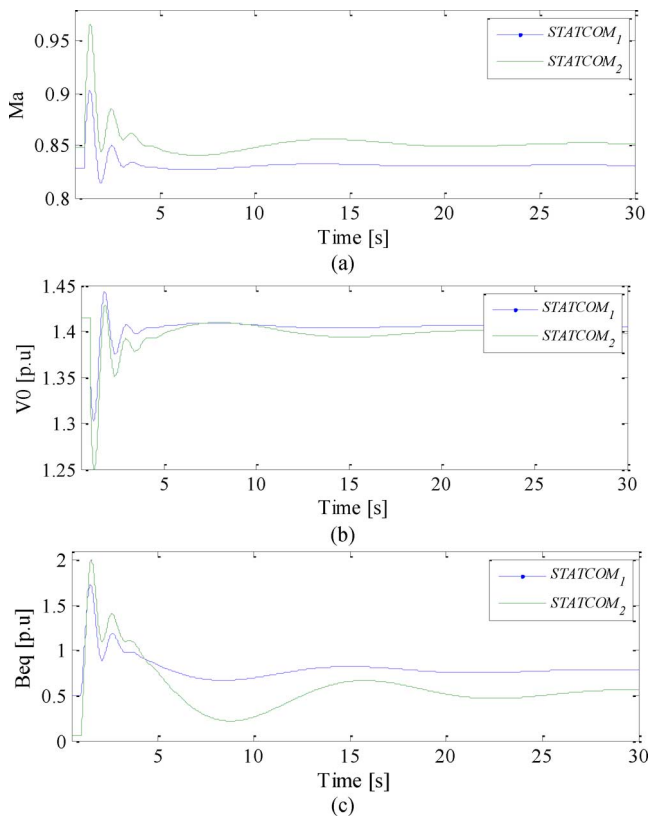

Fig. 11. Results for: (a) modulation index, (b) DC-side voltage and (c) equivalent susceptance.

fast speed of response makes the STATCOM very attractive for power system applications.

Following the disturbance, the modulation index starts to exert voltage control as depicted in Fig. 11(a). Its behavior is governed by (18) from which it can be appreciated that when the terminal voltage V_k is smaller than V_{reg}, the modulation index derivative with respect to time is positive. This explains the increasing values of m_a for both STATCOMs just after the disturbance. Likewise, the equivalent susceptances B_{eq} increase their values in response to the voltage drops at their respective DC buses as shown in Fig. 11(b) and (c). The reason for the sharp increase in B_{eq} can be better understood by referring to (15). This expression states that B_{eq} changes to reflect the variations that take place in the voltage at the DC side, i.e., an increment in its value is obtained when V_0 is less than the reference voltage at the DC side. Moreover, as dictated by (8), a positive change in B_{eq} brings about an increase in the required reactive power output of the STATCOM when a voltage drop is detected at its terminals. The reactive power provided by the VSCs after the transient period reaches approximately 80 and 65 MVAr, respectively, as shown in Fig. 10(c).

It should be noted that the state variables of STATCOM 2 are more sensitive to the disturbance since this STATCOM is located nearer to the transmission line that connects buses 17 and 18, which becomes the only path to supply the large loads connected at nodes 3 and 18. Thus, this device plays a key role in improving the voltage profile at this specific point of the grid.

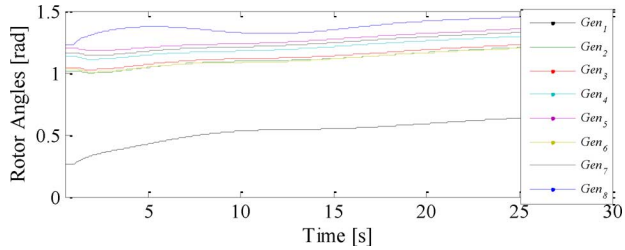

Fig. 12. Generators' rotor angle behavior.

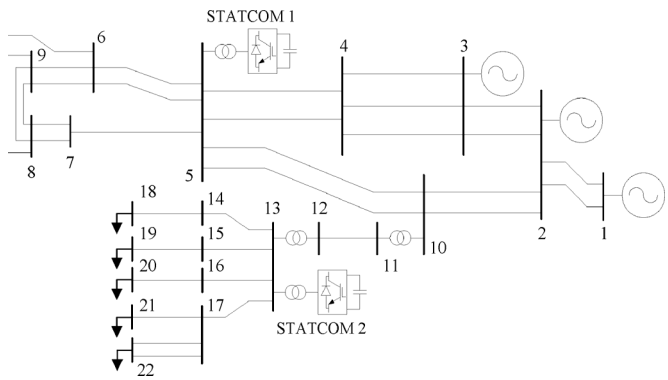

Fig. 13. Relevant area of a realistic power system.

Following the perturbation, a temporary rearrangement of the power flows takes place in the system together with changes in the powers drawn by the loads (owing to their voltage dependency). All this brings about variations in power transfers which are accompanied by changes in the angular separation of the synchronous generators, as shown in Fig. 12.

B. Realistic Power System

A realistic power system which consists of 2172 nodes, 2294 transmission lines, 768 transformers and 160 power plants [13] was used to test further the new STATCOM model. The relevant part of the network depicted in Fig. 13 shows the location of two STATCOMs which are integrated into the network at nodes 5 and 13. This part of the system concentrates a considerably number of power plants which causes the main transmission lines to be highly loaded even during normal operating conditions. STATCOM 1 is located in the main high voltage transmission system corridor and STATCOM 2 is connected in a radial, low voltage system, close to the main load points of this part of the network.

A disconnection of the double circuit connecting buses 5 and 10 causes the voltage to drop very considerably if no dynamic reactive compensation is available, as shown in Fig. 14(a). Assuming that reactive power is provided by the STATCOMs, their steady-state reactive power output stands at -160 MVAr and 30 MVAr in order to control their terminal voltage at 1 p.u. and 1.03 p.u, respectively. As soon as the transmission lines are tripped, the voltages in several nodes of the system start to drop bringing the STATCOMs into operation to regulate dynamically the voltage at their terminals, as shown in Fig. 14(c), reaching

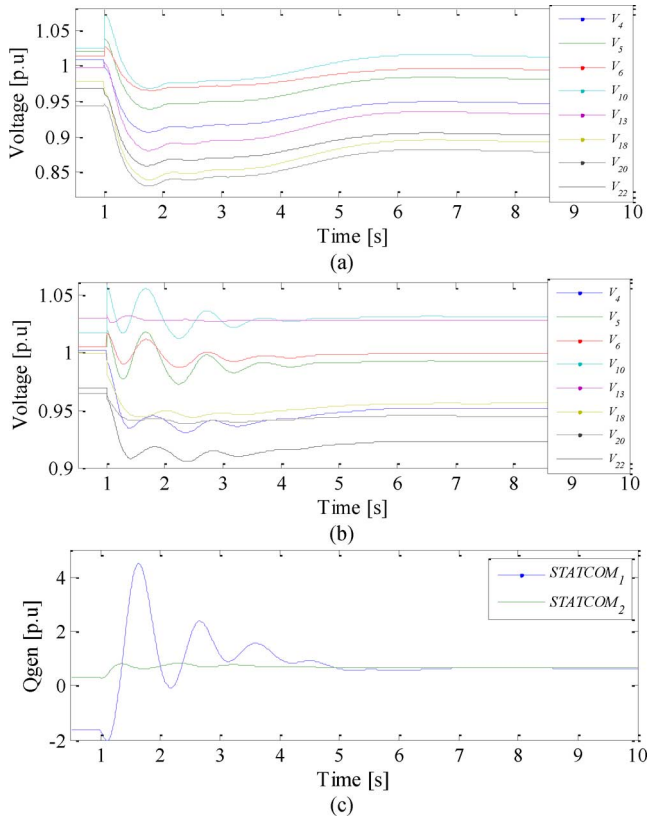

Fig. 14. (a) Voltage behavior with no STATCOMs. (b) Voltage behavior with STATCOMs. (c) Reactive power provided by the STATCOMs.

approximately 450 MVAr and 80 MVAr during the transient period. This reactive power provision helps ameliorate the voltage drop in the affected areas, as can be seen in Fig. 14(b).

These dynamic simulation results show that the new STATCOM model behaves equally well when implemented in a large-scale power grid or when embedded in smaller power systems. This is of paramount importance since power system operators require dynamic models to be reliable regardless of the network size and complexity.

VII. Conclusion

A new STATCOM model for dynamic simulations of large-scale power systems has been put forward in this paper whose modeling concepts do not rely on an equivalent voltage source but rather on the use of a complex phase-shifting transformer as its key element. The model solution is carried out using the Newton-Raphson method which solves simultaneously the algebraic and differential equations at each time step.

A comparative study was carried out to demonstrate that the main output variables and the number of iterations that the new model takes to converge at each time step is consistent with those of a STATCOM model based on conventional voltage source [3]. This is in spite of the modeling approaches being fundamentally different. For instance, the inner active power losses are calculated in a quite different manner and the DC-bus representation in the new STATCOM leads to a much more flexible model. The latter is something that the equivalent voltage source-based model of the STATCOM definitely lacks.

To check further on the robustness of the new model, in what it would represent a more practical situation, a realistic large-scale power system was employed. As expected, its performance was equally reliable as when tested in the small power networks. Generally speaking, the results presented for three test networks show that the STATCOM manages to satisfactorily support the voltage at its point of connection with the power grid and that to a greater or lesser extent, its beneficial effects spread to neighboring nodes.

Appendix A

In connection with Fig. 1(b), the voltage and current relationships in the ideal tap-changing transformer are

$$\frac{\mathbf{V}_1}{\mathrm{V}_0} = \frac{m_a' \angle \phi}{1} \text{ and } \frac{m_a' \angle -\phi}{1} = \frac{\mathbf{I}_2}{\mathbf{I}_1}. \tag{A1}$$

The current through the impedance connected between k and 1 is

$$\mathbf{I}_1' = \mathbf{Y}_1(\mathbf{V}_k - \mathbf{V}_1) = \mathbf{Y}_1\mathbf{V}_k - m_a' \angle \phi \mathbf{Y}_1 \mathrm{V}_0 = \mathbf{I}_k \tag{A2}$$

where $\mathbf{Y}_1 = 1/(R_1 + \mathrm{j}X_1)$. At node 0, the next relationship holds

$$\begin{aligned}\mathbf{I}_0 = -\mathbf{I}_2 + G_{sw}\mathrm{V}_0 = -m_a' \angle -\phi \mathbf{Y}_1 \mathbf{V}_k \\ + m_a^{'2}\mathbf{Y}_1\mathrm{V}_0 + \mathrm{j}B_{eq}m_a^{'2}\mathrm{V}_0 + G_{sw}\mathrm{V}_0.\end{aligned} \tag{A3}$$

Rearranging (A.2) and (A.3) yields

$$\begin{bmatrix}\mathbf{I}_k \\ \mathbf{I}_0\end{bmatrix} = \begin{bmatrix}\mathbf{Y}_1 & -m_a' \angle \phi \cdot \mathbf{Y}_1 \\ -m_a' \angle -\phi \cdot \mathbf{Y}_1 & m_a^{'2}(\mathbf{Y}_1 + \mathrm{j}B_{eq}) + G_{sw}\end{bmatrix} \times \begin{bmatrix}\mathbf{V}_k \\ \mathrm{V}_0\end{bmatrix}. \tag{A4}$$

Appendix B

The implicit trapezoidal method is used to discretize function (19), assuming linearity during the integration time step. The ensuing algebraic equation for the time interval Δt is

$$Y_t = Y_{t-\Delta t} + \frac{\Delta t}{2}(\dot{Y}_{t-\Delta t} + \dot{Y}_t). \tag{B1}$$

Rearranging (B1) as a mismatch equation gives

$$F_Y = Y_{t-\Delta t} + \frac{\Delta t}{2}\dot{Y}_{t-\Delta t} - \left(Y_t - \frac{\Delta t}{2}\dot{Y}_t\right) = 0. \tag{B2}$$

Appendix C

The following parameters are used:

— 9-Node network: 1) Generators: $r_a = 0$ p.u; $X_d = 0.67$; $X_q = 0.62$ p.u; $X_d' = 0.132$; $X_q' = 0.166$ p.u; H $= 4$ s; D $= 0.2$ p.u. 2) STATCOM: Step-up transformer: $X = 0.0586$ p.u; tap $= 1.0253$.

— 39-Node network: 1) Generators: data taken from [13]. 2) STATCOMs: Step-up transformer: $X = 0.06$ p.u; tap $= 1.0$.

— Data for both cases: 1) Turbine-governors: $T_c = 0.3$; $K = 0.06$; $T_w = 0.5$. 2) AVRs: $T_A' = 5$; $K_A = 10$. 3) Loads: $p_p = 0.2$; $p_c = 0.4$; $p_z = 0.4$; $q_p = 0.2$; $q_c = 0.4$; $q_z = 0.4$. 4) STATCOMs: $G_0 = 0.01$ p.u; $R_1 = 0.001$

p.u; $X_1 = 0.01$ p.u; $I_{nom} = 3$ p.u; $K_{dc} = 30$; $T'_{dc} = 0.75$; $K_{ac} = 40$; $T'_{ac} = 0.10$; $K_q = 0.01$; $K_v = 12$.

REFERENCES

[1] N. G. Hingorani and L. Gyugyi, *Understanding FACTS: Concepts and Technology of Flexible AC Transmission Systems*. New York, NY, USA: Wiley-IEEE Press, 1999.

[2] E. Acha, C. R. Fuerte-Esquivel, H. Ambriz-Perez, and C. Angeles-Camacho, *FACTS Modeling and Simulation in Power Networks*. New York, NY, USA: Wiley, 2005.

[3] C. A. Cañizares, "Power flow and transient stability models of FACTS controllers for voltage and angle stability studies," in *Proc. IEEE PES Winter Meeting 2000*, 2000, vol. 2, pp. 1447–1454.

[4] E. Barrios-Martinez, C. Angeles-Camacho, E. Acha, and M. A. Olguin-Becerril, "Dynamic phase-domain modelling and simulation of STATCOM in large-scale power systems," in *Proc. IEEE Power Tech Conf. 2009*, Bucharest, Romania, 2009, pp. 1–9.

[5] S. F. Faisal, A. H. M. A. Rahim, and J. M. Bakhashwain, "A robust STATCOM controller for a multi-machine power system using particle swarm optimization and loop-shaping," *Int. J. Elect. Commun. Syst. Eng.*, pp. 64–70, 2007.

[6] G. Shahgholian, M. Mahdavian, A. Etesami, S. Moalem, and M. Jabbari, "Improvement of dynamic behavior and system stability by using STATCOM," in *Proc. IEEE Int. Symp. Industrial Electronics*, 2011, pp. 1057–1062.

[7] M. Mahdavian and G. Shahgholian, "Effect of STATCOM on enhancing power system dynamic stability," in *Proc. IEEE Int. Conf. Elect. Eng., Comput., Telecomm., and Inf. Technol. (ECTI)*, 2011, pp. 780–783.

[8] K. Wang and M. L. Crow, "Power system voltage regulation via STATCOM internal nonlinear control," *IEEE Trans. Power Syst.*, vol. 26, no. 3, pp. 1252–1262, Aug. 2011.

[9] M. Jabbari, G. Shahgholian, M. Mahdavian, E. Attarpour, and A. Leilaeyoun, "Modeling and dynamic analysis of a STATCOM for system damping enhancement," in *Proc. IEEE Int. Symp. Industrial Electronics*, 2011, pp. 1087–1092.

[10] G. W. Stagg and A. H. El-Abiad, *Computer Methods in Power System Analysis*. New York, NY, USA: McGraw-Hill, 1968.

[11] P. M. Anderson and A. A. Fouad, *Power System Control and Stability*. Ames, IA, USA: Iowa State Univ. Press, 1977.

[12] M. A. Pai, *Energy Function Analysis for Power System Stability*. Norwell, MA, USA: Kluwer, 1989.

[13] F. Aboytes and G. Arroyo, "Security assessment in the operation of longitudinal power systems," *IEEE Trans. Power Syst.*, vol. 1, no. 2, pp. 225–232, May 1986.

[14] M. Rafian, M. J. H. Sterling, and M. R. Irving, "Real-time power system simulation," *Proc. Inst. Elect. Eng., Gen., Transm., Distrib.*, vol. 134, pp. 206–223, May 1987.

[15] H. W. Dommel and N. Sato, "Fast transient stability solutions," *IEEE Trans. Power App. Syst.*, vol. PAS-91, pp. 1643–1650, 1972.

[16] IEEE Committee Report, "Computer representation of excitation systems," *IEEE Trans. Power App. Syst.*, vol. PAS-87, pp. 1460–1464, 1968.

[17] P. Kundur, *Power System Stability and Control*. New York, NY, USA: McGraw-Hill, 1994.

Luis M. Castro received the B.Eng. and M.Sc. degrees from the Instituto Tecnológico de Morelia, Morelia, México, in 2006 and 2008, respectively. He is currently pursuing the Ph.D. degree at Universidad Michoacana. He is currently a visiting Student in the Department of Electrical Energy Engineering of the Tampere University of Technology, Tampere, Finland.

Enrique Acha (SM'02) graduated from Universidad Michoacana in 1979 and received the Ph.D. degree from the University of Canterbury, Christchurch, New Zealand, in 1988.

He was a Professor of Electrical Power Systems at the University of Glasgow, Glasgow, U.K., in the period 2001–2011 and he is now a Professor of Electrical Power Systems at the Tampere University of Technology (TUT), Tampere, Finland.

Claudio R. Fuerte-Esquivel (SM'08) received the B.Eng. (Hons) degree from the Instituto Tecnológico de Morelia, Morelia, México, in 1990, the M.S. degree (summa cum laude) from the Instituto Politécnico Nacional, México, in 1993, and the Ph.D. degree from the University of Glasgow, Glasgow, U.K., in 1997.

Currently, he is a Professor at the Universidad Michoacana, where his research interests lie in the dynamic and steady-state analysis of FACTS.